Lab on a Chip

PAPER

View Article Online
View Journal | View Issue

Cite this: *Lab Chip*, 2025, **25**, 6401

Immune-integrated cardiac fibrosis-on-a-chip: a 3D microfluidic device for region–specific immune–cardiac crosstalk in the fibrotic heart

Jiaying Ji,[ab] Mateo Tristan,[c] Frank Ketchum,[a] Wenzheng Kuang,[d] Guosheng Fu,[d] Xiang Ren[b] and Pinar Zorlutuna *[abc]

Received 12th May 2025,
Accepted 15th October 2025

DOI: 10.1039/d5lc00469a

rsc.li/loc

Cardiac fibrosis following myocardial infarction (MI) is driven by complex interactions among cardiomyocytes (CMs), cardiac fibroblasts (CFs), and immune cells, particularly macrophages. Current *in vitro* models often fail to capture the spatial heterogeneity and dynamic immune–cardiac crosstalk that are central to post-MI remodeling. Therefore, we aimed to develop a physiologically relevant cardiac fibrosis-on-a-chip model that integrates spatially patterned cardiac tissue architecture with region-specific immune cell delivery and mimic post-MI fibrosis. We engineered a three-layer microfluidic device seeded with human iPSC-derived CMs and CFs at defined ratios to replicate scar, border, and healthy regions. A valve-actuation system enabled the controlled introduction of iPSC-derived macrophages (iMacs) in a gradient pattern, mimicking their spatial distribution *in vivo*. TGF-β was used as a comparative biochemical stimulus to establish baseline fibrotic signaling. Immunostaining and computational modeling confirmed the spatial patterning of CM/CF and macrophage gradient distribution. This cardiac fibrosis-on-a-chip model provides an innovative and physiologically relevant system to investigate immune-mediated fibrosis. It enables region-specific analysis of immune–cardiac interactions and serves as a valuable model for therapeutic screening in fibrotic heart disease.

Introduction

Cardiovascular disease (CVD) remains the leading cause of death globally, with a significant increase in death number in recent decades. In 2021, 20.5 million deaths were attributed to cardiovascular disease worldwide, marking a 69.4% rise over the past 30 years.[1] This underscores the critical need for advancing our understanding of CVD mechanisms and treatment strategies. The heart is a highly complex organ, comprising multiple interacting cell types such as cardiomyocytes (CMs), supporting cells like fibroblasts (CFs) and endothelial cells, and immune cells including macrophages and leukocytes. These cells interact dynamically to maintain a healthy cardiac microenvironment.[2]

However, disruptions in this tightly regulated system—such as hypoxia during myocardial infarction (MI)—trigger a cascade of pathological responses.[3,4] These responses include initiation of inflammatory pathways, alterations in cellular metabolism, oxidative stress, excessive extracellular matrix (ECM) deposition and disrupted cardiac cell coupling, ultimately leading to cardiac fibrosis and impairing cardiac function.[5,6] Among immune cells, macrophages have emerged as pivotal players in fibrosis. Following MI, macrophages infiltrate into damaged cardiac regions, polarize into pro-inflammatory phenotypes, and release pro-fibrotic cytokines (*e.g.*, transforming growth factor-beta, TGF-β) to activate CFs into ECM-producing myo-fibroblasts (myo-CFs). Crucially, macrophages exhibit distinct spatial localization within post-MI cardiac tissues: concentrated in the scar to sustain chronic inflammation, while absent in healthy zones to prevent unnecessary fibrosis in the healthy tissue. Additionally, recent research by Hulsmans *et al.*[7] also highlighted the role of macrophages in regulating electrical conduction in the heart by forming gap junctions with CMs. Therefore, accurately replicating immune cell spatial localization and their interactions with cardiac cells *in vitro* is crucial for developing physiologically relevant models.

Traditional 2D cell culture methods fail to replicate the complex three-dimensional architecture and multicellular interactions in the heart,[8] while animal models are limited by species-specific differences, high costs, and the difficulty of interpreting the results due to the complex variables

[a] *Bioengineering Graduate Program, University of Notre Dame, Notre Dame, IN, 46556, USA*
[b] *Department of Aerospace and Mechanical Engineering, University of Notre Dame, Notre Dame, IN, 46556, USA. E-mail: pinar.zorlutuna.1@nd.edu*
[c] *Department of Chemical and Biomolecular Engineering, University of Notre Dame, Notre Dame, IN, 46556, USA*
[d] *Department of Applied and Computational Mathematics and Statistics, University of Notre Dame, Notre Dame, IN, 46556, USA*

involved. As a result, there is a growing demand for simplified yet biomimetic *in vitro* models that can better replicate the native cardiac environment and interactions. Heart-on-a-chip systems have emerged as promising alternatives, but most focus solely on CMs–CFs interaction or the introduction of biochemical factors (*e.g.*, TGF-β), without incorporating immune components. For instance, Jaimeson Veldhuizen *et al.*[9] developed an ischemia-on-chip microfluidic model composed of a collagen-based hydrogel, CMs, and CFs, that can recapitulate post-ischemia cardiac fibrosis through exposure to a controlled hypoxic environment, but did not include immune cells integration. Similarly, Erika Yan Wang *et al.*[10] proposed a new biowire model that exploits wire deflection to measure the contractility and electrical properties of healthy and fibrotic cardiac tissue and investigate the interaction between a fibrotic region and the adjacent healthy tissue; however, their model did not incorporate macrophage-driven fibrosis. Other platforms have used uniform TGF-β stimulation to induce fibrosis, but these approaches do not reflect the heterogeneity and spatial organization observed *in vivo*. These limitations underscore the need for an *in vitro* model that integrates both immune dynamics and localized fibrotic microenvironments.

In this paper, we developed a three-dimensional (3D) cardiac fibrosis-on-a-chip model (Fig. 1a) that advances existing models by incorporating immune cells with spatially patterned scar, border, and healthy cardiac tissue regions, thereby closely mimicking the heterogeneous tissue architecture of post-MI fibrosis (Fig. 1b). Our model is built on a three-layer microfluidic device (Fig. 1c) and utilizes human-induced pluripotent stem cells (iPSCs)-derived cardiomyocytes (iCMs) and iPSC-derived cardiac fibroblasts (iCFs) to recapitulate scar, border, and healthy regions of the heart through precise spatial patterning of CM and CFs (Fig. 1d), enabling region-specific cellular compositions and direct multicellular interactions. The key innovation of our device is the valve actuation system, which enables precise delivery of iMacs to mimic their gradient distribution *in vivo*—densely concentrated in the scar and decreasing toward the healthy region (Fig. 1e). The presence of iMacs in the scar region enabled the creation of a hyperinflammatory microenvironment for investigating macrophage-mediated cardiac fibrosis. We introduced a gradient of TGF-β to establish a baseline fibrotic environment for comparison with more complex macrophage-mediated effects. Our immunostaining results validated the distinct CM/CF ratios and the expression of CM/CF markers across regions. Computational modeling and experimental data further demonstrated gradient macrophage distributions across the scar-border-healthy regions, replicating post-MI immune dynamics. To our knowledge, this is the first cardiac fibrosis-on-a-chip model to combine immune cell spatial localization with engineered fibrotic tissue architecture. By bridging these gaps, our device provides a more physiologically relevant system for investigating the interplay between immune cells and fibrosis progression and offers a powerful tool for

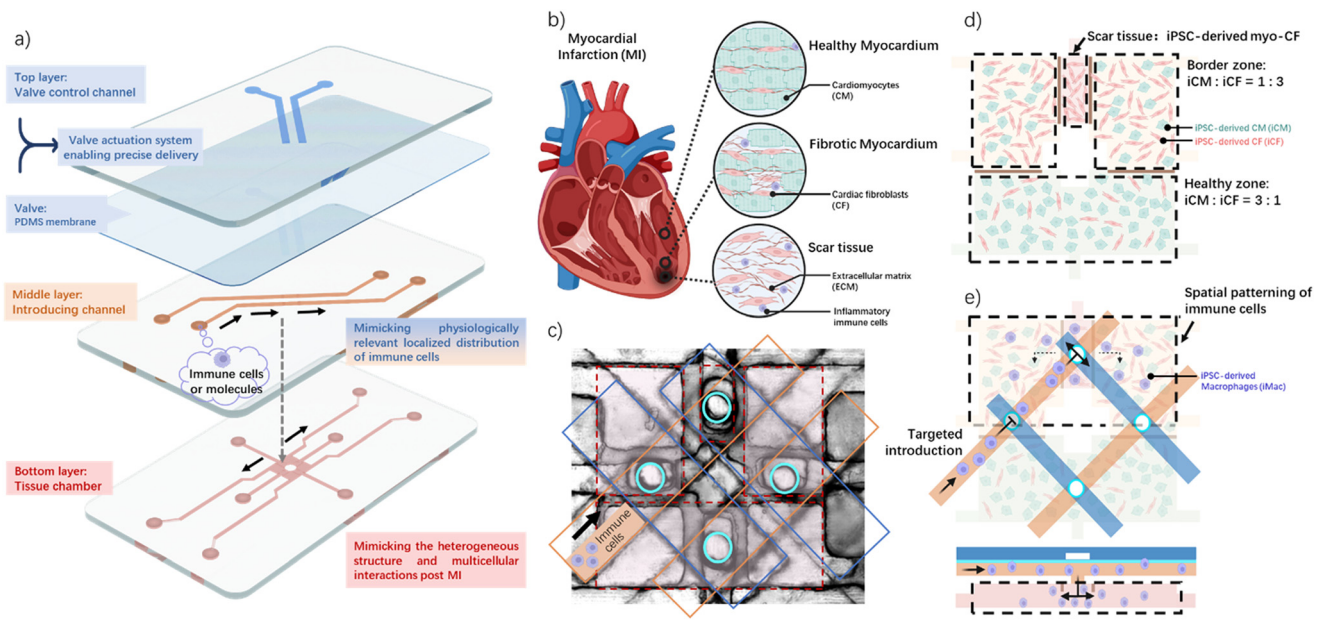

Fig. 1 Design and function of a microfluidic heart-on-a-chip model to study region-specific immune-mediated cardiac fibrosis. (a) Schematic of the three-layer microfluidic device: the top and middle layer control the spatial introduction of immune cells and other biochemical cues, and the bottom tissue layer achieves 3D cell-patterning. (b) Schematic of the heterogeneous architecture of post-MI tissue, including scar tissue, fibrotic border myocardium, and healthy myocardium. (c) The real brightfield image of the three-layer microfluidic device. (d) Schematics illustrating the co-culture of iCMs and iCFs to mimic the heterogeneous tissue architecture in post-MI. (e) Schematics illustrating the spatial introduction of immune cells (*i.e.*, iMacs) to mimic the spatial distribution of immune cells in post-MI.

evaluating potential therapeutic strategies within localized cardiac microenvironments.

Materials and methods

Cardiac fibrosis-on-a-chip device design and fabrication

The cardiac fibrosis-on-a-chip device comprises three polydimethylsiloxane (PDMS) layers fabricated using 3D wax printing and PDMS casting, analogous to standard soft lithography. A schematic diagram and a photograph of the microfluidic device are shown in Fig. 1a. The bottom layer enables precise cell patterning *via* stepped height. This layer contains eight interconnected tissue chambers (800 μm × 800 μm or 300 μm × 800 μm), semi-separated by the physical barriers. The chambers and barriers had stepped heights: the tissue chamber height was 300 μm while the barrier height was 100 μm in height. The stepped height prevented the hydrogel spreading and refined the distribution of the hydrogel during seeding. As cells cultured over time, the adjacent hydrogel compartments gradually interconnected with each other. Each chamber connects to an individual seeding channel, enabling targeted hydrogel seeding and flexible cell patterning for the cardiac fibrosis-on-a-chip device.

The middle layer functions as a valve actuation system with the top layer, guiding biochemical cues (*e.g.*, soluble molecules and external cells) to specific target locations. The middle layer includes two introducing channels and four outputs, which are positioned above tissue chambers. The top layer controls the allowance or suspension of the biochemical cues in the middle layer. Such controlling in the top layer operates *via* pneumatic actuation. The top layer consists of two valve control channels and a thin PDMS membrane. When pressure is applied to the valve control channels, the membrane bends downward, allowing or suspending the flow of cell- or molecule-laden fluids in the introducing channels, ensuring precise biochemical cue delivery.

For fabrication, microchannel designs for all layers were drafted using computer-aided design software, and molds were 3D-printed in wax (Solidscape, Inc). PDMS (Sylgard 184, 10 : 1 base-to-curing agent ratio) was poured into the molds, degassed, and cured at 80 °C for 2 hours. The spin-coated PDMS membrane and fabricated layers were bonded sequentially *via* oxygen plasma treatment (120 seconds) and pressed onto a glass substrate.

iPSC culture and induced cardiomyocyte (iCM) differentiation

In the DiPS 1016 SevA (male dermal fibroblast-derived iPSC) iPSC line, iPSCs were differentiated into iCMs using a modified protocol[11] for improved metabolic maturation. On days 0–1, iPSCs at 95% confluency were treated with CM (−) medium (RPMI 1640 supplemented with 2% B27 minus insulin, 0.1 mM β-mercaptoethanol, and 1% penicillin–streptomycin) containing 10 μM CHIR99021. From days 2–3, media was replaced with CM (−) + 2 μM CHIR99021, followed by treatment with CM (−) + 5 μM Wnt inhibitor IWP-4 on day 4. On day 6, media was switched to CM (−), and from day 9 to day 12, cells were maintained purification media (RPMI 1640 without glucose supplemented with 2% B27 and 1× FA-BSA). Starting from day 17, cells were maintained in metabolic maturation media. The metabolic maturation media was based on RPMI without glucose (Thermo Fisher Scientific, 11966025), supplemented with 3 mM glucose (Sigma Aldrich, G7021), 10 mM L-lactate (Sigma Aldrich, 71718), 5 μg ml^{-1} vitamin B12 (Sigma Aldrich, V6629), 0.82 μM biotin (Sigma Aldrich, B4639), 5 mM creatine monohydrate (Sigma Aldrich, C3630), 2 mM taurine (Sigma Aldrich, T0625), 2 mM L-carnitine (Sigma Aldrich, C0283), 0.5 mM ascorbic acid (Sigma Aldrich, A8960), 1× NEAA (Thermo Fisher Scientific, 11140), 0.5% (w/v) Albumax (Thermo Fisher Scientific, 11020021), 1× B27 and 1% KOSR (Thermo Fisher Scientific, 10828028). Cell media was refreshed every 3 days. Beating iCMs were typically observed by day 21.

iPSC culture and induced cardiac fibroblasts (iCF) differentiation and myo-iCF transdifferentiation

A previously published differentiation protocol[12] was adapted for CF differentiation from iPSCs.45 At 100% confluency, iPSCs were treated with CM (−) supplemented with 10 μM CHIR99021. After 24 h, the media was replaced with CM (−) without CHIR. On day 3, the media was changed to cardiac fibroblast differentiation basal medium supplemented with FBS (10% Hyclone), containing 75 ng mL^{-1} FGF, and this process was repeated every other day until day 20. On day 20, the tissue culture flask was coated with fibronectin (Sigma Aldrich) in phosphate-buffered saline (PBS) (50 μg mL^{-1}). The iCFs were then detached using trypsin-EDTA (0.25%, Stem Cell Technologies) and passaged on these flasks and cultured in DMEM (Dulbecco's modified Eagle's medium) high glucose media (4.5 g L^{-1}, basal medium, Corning) supplemented with FBS (10%), penicillin–streptomycin (P/S, 1%) (Sigma), and SD208 (3 μM, TGF-β receptor 1 kinase inhibitor) (Sigma-Aldrich, St. Louis). iCFs were maintained with media changes with SD208 (3 μM) added DMEM high glucose media supplemented with FBS (10%) and P/S (1%) (DMEM complete) every 2 days and kept at 37 °C with 5% CO_2. For myo-iCF differentiation induction, iCFs were treated with DMEM high glucose media supplemented with TGF-β (10 ng mL^{-1}, Abcam) when they were around 80% confluency. myo-iCF were maintained with media changes using DMEM complete every 2 days and kept at 37 °C with 5% CO_2. The success of the differentiation and transdifferentiation has been confirmed using immunofluorescence-specific markers in our lab previously.

iPSC culture and induced macrophages (iMac) differentiation

A previously published differentiation protocol[13] was adapted for iMac differentiation from iPSCs. This protocol utilized the spontaneous differentiation of iPSC into embryoid bodies

(EB), followed by directed differentiation along the myeloid lineage by IL-3 and M-CSF, to produce a homogeneous population of monocytes, which can be further differentiated into macrophages (iMac). For EB formation, mechanical dissociation was employed: iPSCs were mechanically dissociated by scoring each 10 cm^2 well into a grid of ~100 patches using a 23G needle. The patches were lifted with a cell scraper, transferred to a 6-well ultra-low adherence plate (Corning) in iPSC culture medium, and cultured for 4 days. EBs (~10 per 6-well plate or 1 per 24-well plate) were cultured in X-VIVO™ 15 medium (Lonza) supplemented with 100 ng mL^{-1} M-CSF (Invitrogen), 25 ng mL^{-1} IL-3 (R&D Systems), 2 mM GlutaMAX (Invitrogen), 100 U mL^{-1} penicillin, 100 μg mL^{-1} streptomycin, and 0.055 mM β-mercaptoethanol. Two-thirds of the medium was replaced every 5 days. Once monocytes were visible in the supernatant of the cultures (from 2–3 weeks onwards), non-adherent monocytes were harvested weekly from the supernatant of EB cultures. Monocytes were plated onto tissue culture-treated 6-well plates (Corning) at a density of 1.5 × 106 cells per well. Monocytes were maintained in X-VIVOTM15 medium (Lonza) supplemented with 100 ng mL^{-1} recombinant human M-CSF (R&D Systems), 2 mM glutamine (PAA), 100 U mL^{-1} penicillin and 100 μg mL^{-1} streptomycin (PAA). Monocytes were incubated at 37 °C, with 5% CO_2 and differentiated for 5–7 days prior to use. IFNγ (R&D, 100 U mL^{-1}) and LPS (Sigma, 100 ng mL^{-1}), or IL-4 (50 ng mL^{-1}, R&D) were added to the culture medium for activation of macrophages.

Cell localization identification in the cardiac fibrosis-on-a-chip

Cell tracker. Differentiated cells were collected using trypsin-EDTA and tagged with cell trackers before seeding. iCMs were labeled with CellTracker Green CMFDA (1 μM, Life Technologies), iCFs were labeled with CellTracker Deep Red (1 μM, Life Technologies), and iMacs were labeled with CellTracker Blue (1 μM, Life Technologies) dyes following the manufacturer's instructions. After seeding into the chip and culturing, the tiled images were taken and stitched together using a fluorescence microscope (Zeiss, Hamamatsu ORCA flash 4.0).

Immunostaining. Immunostaining was performed on the chip to show the cell-specific protein expression in different regions. Briefly, after culturing 7 days, the chip was washed twice using PBS and fixed with paraformaldehyde (4%, Electron Microscopy Sciences) for 1 hour for at room temperature, and then washed with PBS for 30 minutes with washes every 10 minutes. Cells were permeabilized by incubation in Triton X-100 (0.1%, Amresco) solution for 45 minutes and then washed with PBS three times every 10 minutes, for a total 30 minutes. Then, goat serum (10%, Sigma-Aldrich) was used to block the cells for 2 hours at room temperature, and cells were incubated with desired primary antibody diluted according to the manufacturer's recommendations at 4 °C overnight. iCMs were marked with troponin-T, iCFs with vimentin and myo-iCF with alpha-SMA (Abcam). The chip was then washed with PBS, and incubated with secondary antibodies, 647-rabbit (Abcam) and 488-mouse (Abcam), diluted (1 : 200) in goat serum at 4 °C for 6 hours. The chip was then washed with PBS three times and incubated with DAPI (1 μg mL^{-1} w/v in PBS, Sigma-Aldrich) for 5 min at room temperature. The washing process with PBS was repeated until no background remained. Finally, imaging was performed with confocal fluorescence microscopy. Post imaging processing was performed using the Zeiss Zen software and ImageJ (National Institutes of Health).

COMSOL simulation for shear stress of PDMS valve

COMSOL Multiphysics software was used to simulate the shear stress and the deformation of the PDMS valve. PDMS is generally regarded as an isotropic, incompressible, hyperplastic material. We used one of hyperplastic constitutive models, neo-Hookean model, to predict the small and medium deformations under external loading.[14] Boundary conditions included constraining all four edges of the PDMS valve, with a centrally applied external force, ranging from one atmosphere to five atmospheres (*i.e.*, 1 × 10^5 to 5 × 10^5 N m^{-2}). The dimensions of the simulation geometry were 400 μm × 500 μm × 15 μm, closely approximating the actual PDMS valve dimensions.

COMSOL simulation for molecule's gradient distribution

COMSOL Multiphysics software was used to simulate the targeted introduction of small molecule and their gradient distribution within the microfluidic devices. The simulation model integrated transient convection–diffusion equations coupled with the Stokes flow equations, omitting the inertial terms due to the low Reynolds numbers in microfluidic systems. The diffusion coefficient (D = 6 × 10^{-11} m^2 s^{-1}) within the collagen matrix was adopted from previously published data.[15,16] In microfluidics devices, boundary conditions included constant source and sink conditions, a flow velocity of u = 0.05 μm s^{-1}, to model the delivery of soluble molecules from the input of introducing channels with a zero relative pressure flow condition at the outlets. The velocity field from the creeping flow module was utilized in the diluted species transport module. Simulations were executed in two sequential stationary steps: the first step established steady-state creeping flow, while the second step modeled the steady-state transport of molecular species within the established flow conditions.

Statistical analysis

Data were represented as average ± standard error of the mean (SEM), when specified. The one-way analysis of variance (ANOVA) with Tukey's *post hoc* was used to find any statistically significant differences. If there were two individual groups, the Student's *t*-test was performed. All p values were reported to be two-sided, and $p < 0.05$ was

considered statistically significant. Sample size (n) = 3 for all individual experiments.

Results

Our cardiac fibrosis-on-a-chip was designed to replicate the heterogeneous tissue architecture post-MI (scar, border, healthy regions) by controlling the precise spatial patterning of iCMs, iCFs and iMacs. A key innovation of our system is the targeted delivery of immune cells to fibrotic regions, mimicking their *in vivo* distribution: densely localized within scar zones and sparse in healthy tissue. Unlike prior models primarily focusing on TGF-β stimulation to induce fibrosis, our model co-patterns immune cells with cardiac cells, allowing for a more physiologically relevant model of post-MI remodeling. This design enables the investigation of immune cell-mediated fibrosis and captures dynamic macrophage–CM/CF interactions—such as gap junction formation and paracrine signaling—that are absent in TGF-β-centric systems.

Spatial cell patterning to replicate post-MI tissue architecture

To recapitulate the distinct cellular interactions and heterogeneous structure of the scar, border, and healthy regions observed in post-MI hearts, we implemented a spatial cell-patterning method using microfluidic features in the bottom layer of our device.

This spatial cell-patterning method in the bottom layer relies on the stepped heights of tissue chambers and leverages the capillary burst valve (CBV) effect.[17] The CBV effect refers to the phenomenon in which a liquid within a microchannel becomes trapped when it encounters a sudden expansion in channel width. In our microfluidic device, the stepped heights of tissue chambers provide the abrupt dimensional change necessary to confine the hydrogel exclusively to the seeding chambers.

To validate this spatial patterning, we introduced two types of cell-laden hydrogels into different chambers using fluorescent cell trackers for visualization (Fig. 2). Fibroblasts were used here as the cell source. First, green-labeled cells were seeded into the side chambers. After gelation, red-labeled cells were introduced into the central interconnection chamber. The results confirmed that the two cell-laden gels remained successfully separated, illustrating the capability of patterning multiple cell populations with spatial precision, and replicating the organization of scar, border, and healthy zones in post-MI hearts.

Valve actuation system

The valve actuation system, a central feature of the microfluidic device, enables selective TGF-β stimulation and the targeted delivery of immune cells to specific tissue regions.

This system integrates the introducing channels in the middle layer, which direct TGF-β and external immune cells to targeted sites, and the valve control channels in the top layer, which use pneumatic actuation to alter the valves' states, thereby permitting or inhibiting fluid flow within the introducing channels and controlling the delivery area of TGF-β and introduced immune cells.

The criss-cross arrangement of the introducing and valve control channels serves two purposes: first, to maximize optical access to the bottom tissue chambers for subsequent microscopic measurements, and more importantly, to enable independent regulation of each valve under different inputs, thereby allowing precise selection of target tissue chambers and control of delivery areas. Delivery into a target tissue chamber depends on the open state of the corresponding valve (Fig. 3a). A table summarizing the opening valves under different input conditions is provided in Fig. 3b, where "1" and "0" represent actuated and non-actuated channels, respectively. For example, when introducing channel A and

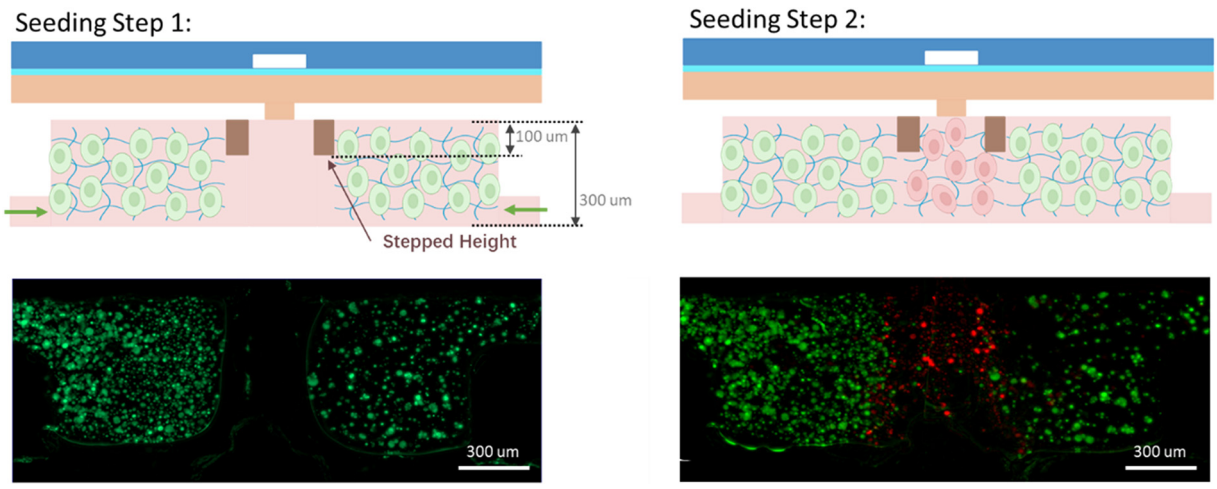

Fig. 2 The schematic and immunostaining demonstration of two-step seeding and the resulting separate cell patterns using two different cell-trackers. Fibroblasts were used here as the cell source. The top row presents cross-sectional views, while the bottom row shows top views.

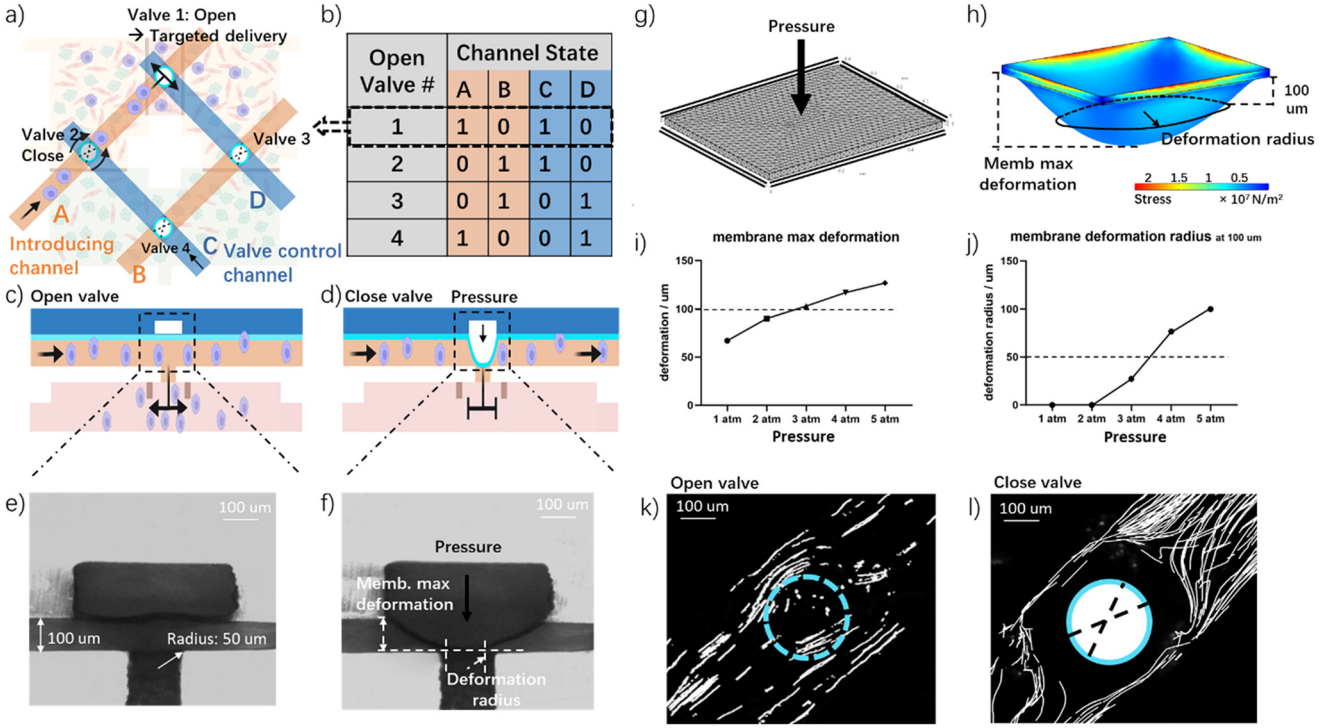

Fig. 3 The valve actuation system for targeted introduction. (a) The schematic for valve actuation system for targeted introduction. The valve 1 is at open state, achieved by the actuation of the related introduction channel A and the non-actuation of the valve control channel D. The valve 2 is at close state, achieved by the actuation of the valve control channel C. (b) A table for the conditions for opening each valve: "1" stands for the actuation of the related channel, while "0" stands for non-actuation. (c and d) The cross-section schematic showing the open and close state of the pneumatic valve and the target introduction. (e and f) The cross-section brightfield images showing the open and close state of the pneumatic valve. (g) The simulation model and domain meshing of the thin PDMS membrane. (h) Simulated shear stress generated in COMSOL, with color gradients representing varying stress levels on the PDMS membrane. (i) The membrane maximum deformation under different pressure conditions. (j) The membrane deformation radius at height of 100 um under different pressure conditions. (k and l) Experimental demonstration of non-obstructed flow with an open valve and the obstructed flow with a close valve by tracking the particle movements in introducing channels.

valve control channel C are actuated, valve 1 remains in the open state, delivering the TGF-β or immune cells to the tissue chamber beneath valve 1, while the other three valves remain closed. If the input changes—for instance, when channels B and C are actuated—valve 2 becomes the only open valve, and the delivery area is redirected accordingly. In this way, the criss-cross channel design allows independent regulation of each valve and spatial control of the delivery area.

The valve mechanism operates as follows:

Open state: the introduction channel is actuated while the valve control channel remains non-actuated, permitting unrestricted flow to the target chamber (Fig. 3c, e and k).

Closed state: the introduction channel is blocked due to PDMS membrane deformation, preventing the delivery of biochemical cues to the target cell chamber. (Fig. 3d, f and l).

Valve states were controlled by pressure-induced PDMS membrane deformation (Fig. 3c and d). The inherent elasticity of the PDMS facilitates its deformation, consequently blocking the introduction channel under pressure and switching the valve states.

To characterize membrane deformation under varying pressures, we conducted simulations of deformation and shear stress using the COMSOL software (Fig. 3g). The model implemented in the simulation was designed as a thin PDMS membrane with a thickness of 15 μm. The boundary conditions were such that all four edges of the membrane were constrained, while a uniform pressure load was applied across the membrane's surface. The results (Fig. 3h) confirmed a spherical deformation pattern consistent with our hypothesis. Further simulations under pressures ranging from 1 to 5 atmospheres (Fig. 3i and j) indicated a non-linear displacement trend, consistent with PDMS's non-linear elastic properties. To achieve complete valve closure, two conditions had to be satisfied: the maximum membrane deformation needed to exceed 100 μm, and the deformation radius at 100 μm depth had to be greater than 50 μm to effectively block the introducing channel. Based on these conditions, a pressure of 4 atmospheres was determined to be the minimum required for a full valve closure.

We performed a demonstration experiment using fluorescent-labeled cells introduced through the introducing channel under both open and closed valve conditions. The cell tracking are shown in Fig. 3k and l. When the valve remained open, the introduced cells flowed freely through the channel and were delivered into the targeted bottom cell chamber. Conversely, when applying pressure to the top

control channel, the PDMS membrane deformed and effectively blocked the introducing channel, preventing cell delivery to the bottom chambers.

Immune integration: gradient-based introduction of macrophages. The key innovation of our microfluidic device is the precise introduction of external immune cells into targeted regions, which allows us to investigate how localized immune infiltration influences cardiac remodeling and fibrosis after MI. By manipulating fluid outflows, we can direct cell-laden flows exclusively to specific chambers. For example, introducing cells into a single target chamber requires adjusting outflows to confine flow passage exclusively to that chamber (Fig. 4a). Similarly, distributing cells into multiple chambers involves keeping multiple outflows open, guiding cells into multiple target regions (Fig. 4d).

To verify the device design and demonstrate the controlled delivery area of introduced cells, we used a finite element method to simulate the fluid motion which is governed by the Stokes equation, where the Reynolds number of the fluid is trivial thus the convection term is negligible. Here we employed the H(div)-conforming hybrid discontinuous Galerkin (HDG) method, which is stable, high-order accurate, mass-conserving, and pressure-robust. The linear system of the numerical scheme is solved with static condensation and geometric multigrid preconditioners recently developed in recent studies,[18,19] and the computational cost is significantly reduced to assist with the design verification. As shown in Fig. 4b, when a single outflow in the tissue chambers is open and cell-laden flow is guided to this specific cell chamber, the simulation indicated that the flow — and thus the cells within it — will be exclusively confined to the chamber associated with the open outflow. Experimental validation using cell tracking revealed that introduced cells predominantly localized within the designated target chambers, confirming simulation results (Fig. 4c). When multiple outflows were opened, introduced cells were effectively distributed among the corresponding chambers (Fig. 4e and f). These findings demonstrate the effectiveness of our valve actuation system in manipulating cellular delivery, enabling controlled studies on iCM and iCF responses to external cellular stimuli.

TGF-β selectively stimulation: a gradient TGF-β concentration

TGF-β is a key cytokine in modulating cellular behavior and promoting ECM remodeling during cardiac fibrosis. Exogenous TGF-β was commonly used as a disease stimuli in the fibrotic disease models. In our model, we introduced TGF-β as a control group to represent fibrotic activation in the absence of immune cell dynamics. Utilizing the valve actuation system, our microfluidic device enables the targeted introduction of TGF-β and the formation of a spatial concentration gradient within defined regions of the cardiac fibrosis-on-a-chip.

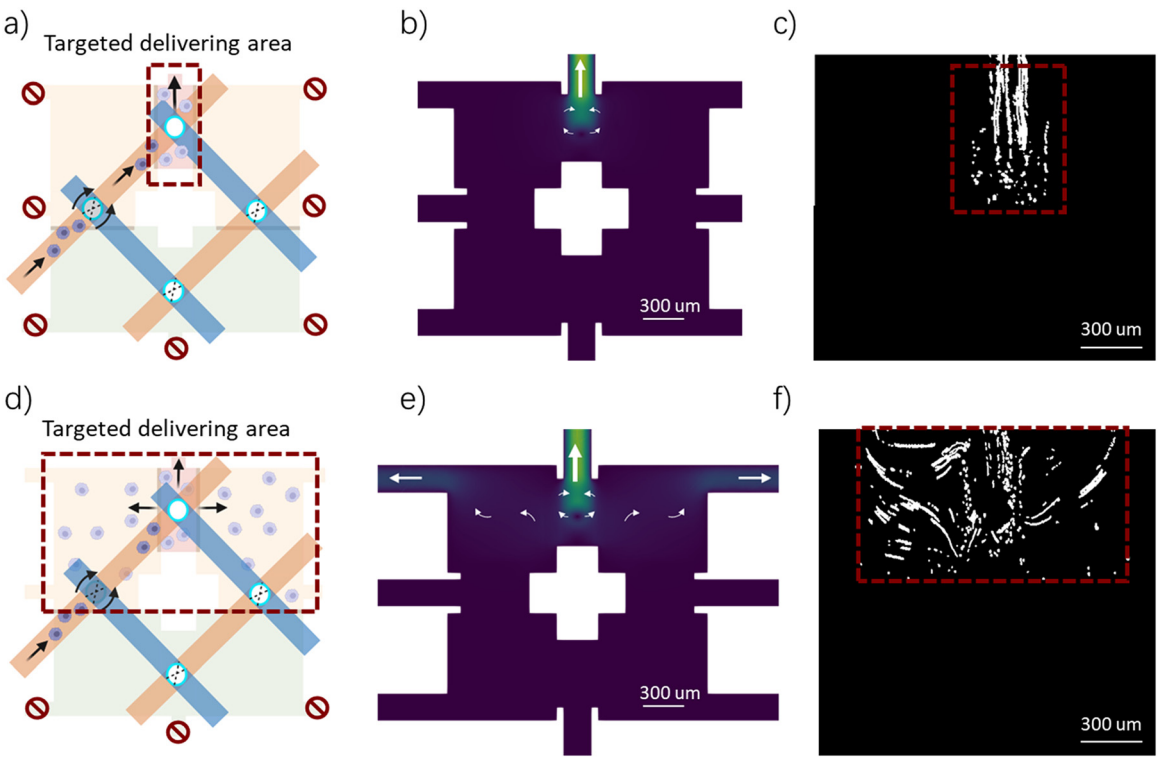

Fig. 4 Targeted introduction of biochemical factors: immune cells with controlled delivery area. (a and d) The schematic of controlling distribution of the cell-laden flows with one or three outflow. (b and e) Simulation results based on a finite element method to verify the flow motion. (c and f) Experimental demonstration of the flow motion by tracking the movements of labeled cells with one or three outflow. Fibroblasts were used here as the cell source.

To achieve this, we continuously perfused a TGF-β-containing solution through the designated introducing channel, while the downstream tissue chambers were pre-filled with molecule-free medium, thereby establishing a stable concentration difference. This source-sink mechanism creates a stable concentration gradient, with the highest TGF-β levels near the introduction site and progressively decreasing concentrations across the adjacent regions.

To verify this gradient formation, we conducted computational simulations using COMSOL to model molecular diffusion within the microfluidic device (Fig. 5b). In this simulation, a high concentration of soluble molecules was introduced through the designated introducing channel, represented by red, while each cell chamber's end was filled with a molecule-free medium, shown in blue. The steady-state simulation results in Fig. 5b display a concentration gradient across the tissue chambers, which are in agreement with our hypothesized behavior of the gradient TGF-β distribution. Experimental validation was performed using a fluorescent dye to mimic biomolecule diffusion (Fig. 5c). The quantitative fluorescence intensity profile confirmed a concentration gradient that closely matched the simulation predictions (Fig. 5d and e).

These findings demonstrate that our valve actuation system and microfluidic device can reliably generate spatial gradients of TGF-β, selectively stimulating the scar and border fibrotic regions in our model. This gradient-based delivery replicates the localized TGF-β expression observed in fibrotic scar tissue, establishing a controlled fibrotic baseline for comparison with immune cell-mediated remodeling. Moreover, the success of our gradient delivery system highlights its capability to replicate physiological biomolecular distributions within fibrotic cardiac tissue and to facilitate *in vitro* studies of spatially regulated cellular responses to growth factors, cytokines, and other signaling molecules in cardiac fibrosis.

Cardiac fibrosis-on-a-chip model with targeted biochemical factors

We utilized the cardiac fibrosis-on-a-chip to model the pathological cardiac fibrosis tissue after MI. First, we employed the spatial cell-patterning method in the bottom layer to recapitulate the three regions of fibrosis observed in

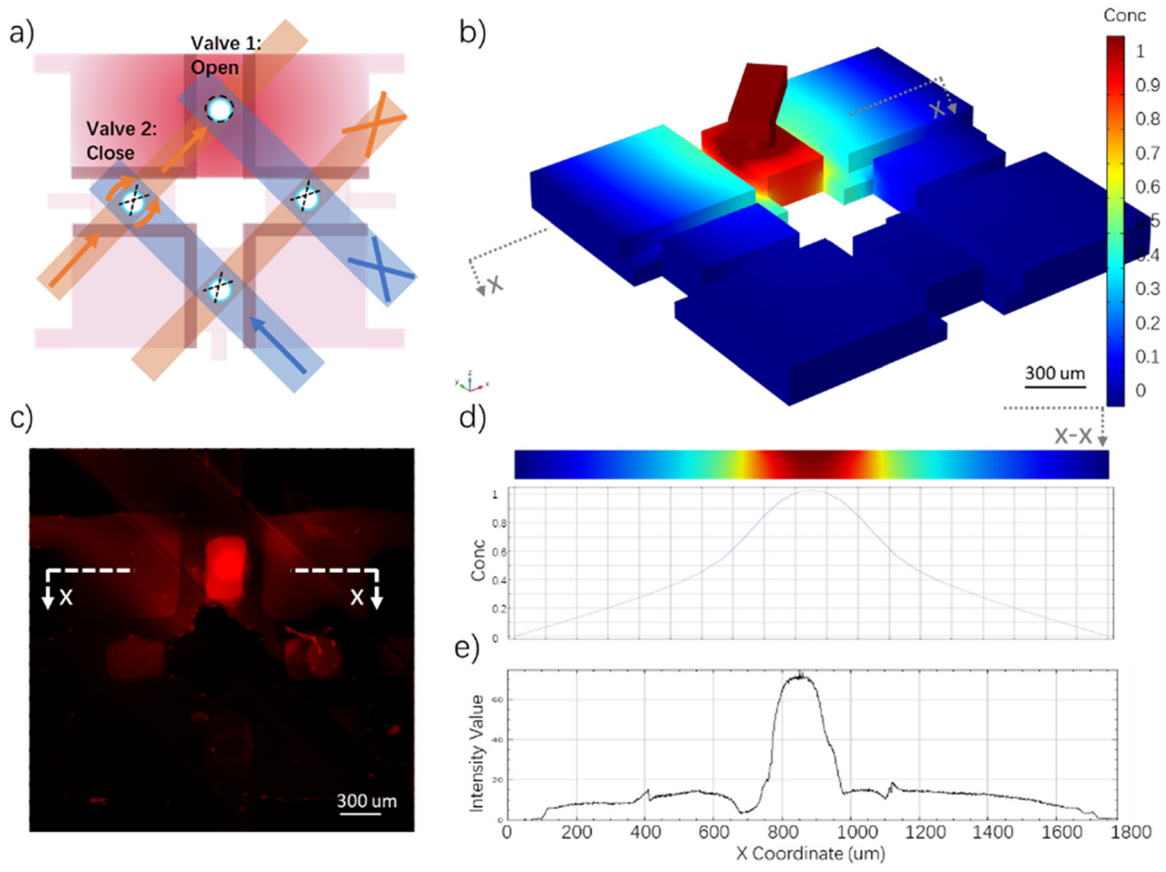

Fig. 5 Targeted introduction of biochemical factors: biomolecules with a gradient delivery. (a) The schematic of implementing a gradient delivery system for molecules. (b) Simulated concentration generated in COMSOL, with color gradients representing varying concentration levels in the microfluidic device. (c) The experimental demonstration of gradient concentration using a fluorescent dye. (d and e) The histogram of concentration at *x*–*x* plane in simulation and the fluorescent dye intensity in experimental demonstration.

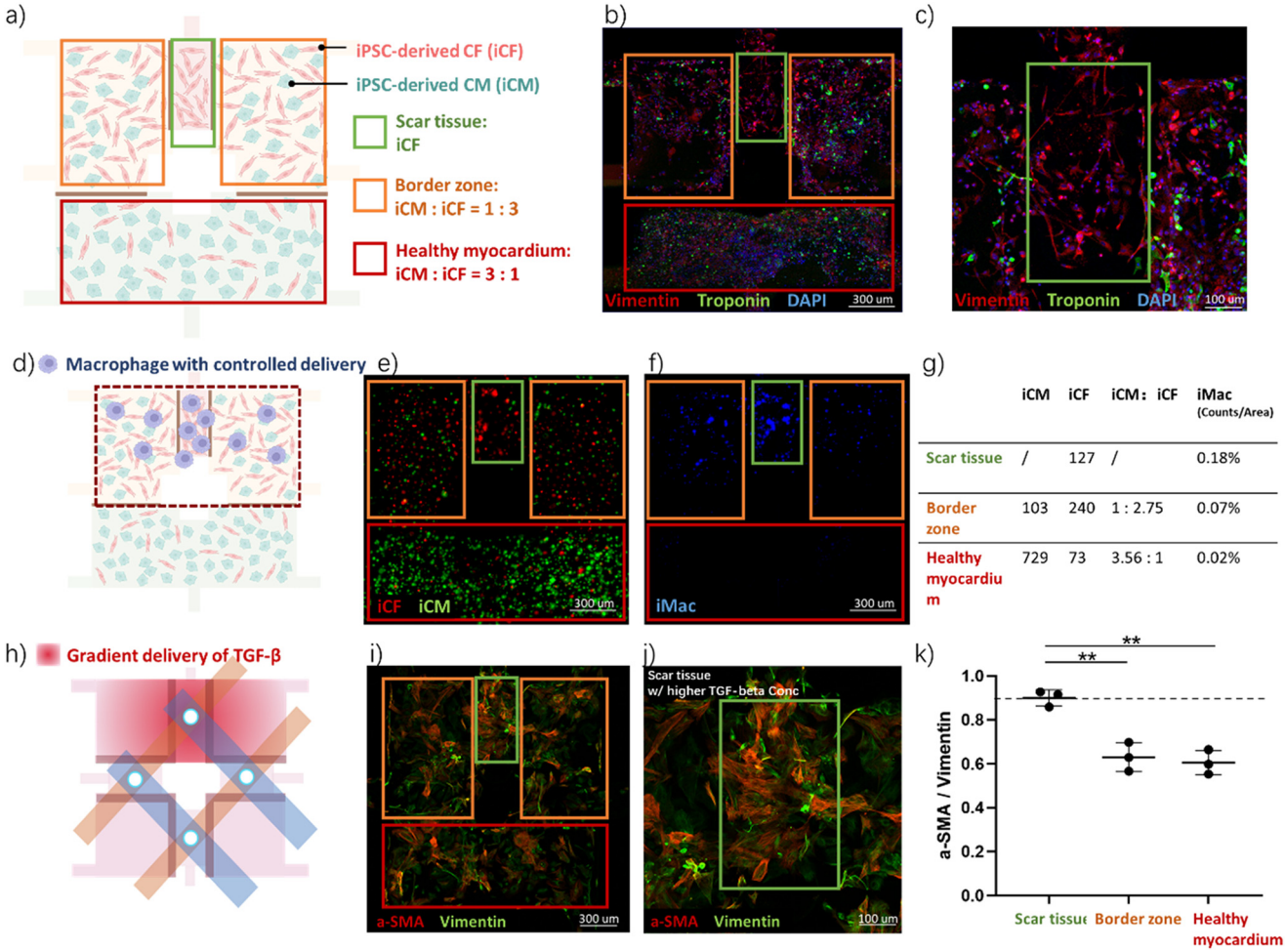

Fig. 6 Cardiac fibrosis-on-a-chip model with targeted biochemical factors. (a) The schematic of employing the spatial cell-patterning method in the bottom layer to recreate the three distinct regions of fibrosis observed in post-MI hearts: scar tissue, border zone, and healthy myocardium. (b and c) Immunostaining results of our cardiac fibrosis model using cell-specific biomarkers—troponin-T for iCMs and vimentin for iCFs. (d) The schematic of introducing macrophages with a gradient distribution. (e and f) The cellular distribution of iCF (red), iCM (green) and macrophage (blue) in our cardiac fibrosis model. (g) The quantification results of cell amount in the scar, border and healthy sections. (h) The schematic of introducing TGF-β with a gradient concentration. (i and j) Demonstration of the gradient concentration of TGF-β by comparing the ratio of alpha-SMA (red) to vimentin (green). (k) The quantification results of the ratio of alpha-SMA staining to vimentin in scar tissue, border and healthy sections (n = 3, $^{**}P \leq 0.01$).

post-MI hearts: scar tissue, border zone, and healthy myocardium (Fig. 6a and c). To incorporate the immune cells to fibrosis progression, we introduced macrophages with controlled spatial localization, achieving a distribution that mirrors *in vivo* conditions—highly concentrated in the scar region and gradually decreasing toward the healthy myocardium. As a control condition to assess fibrotic activation independent of immune cell involvement, we introduced TGF-β in a gradient pattern, with the highest concentration in the scar region and lower concentrations in surrounding areas.

A. Cell-patterning in cardiac fibrosis. To achieve cell patterning of cardiac fibrosis, iPSCs were differentiated into iCMs and iCFs following established protocols,[20] with the phenotypic and functional properties of the differentiated cells previously validated by our lab. To accurately mimic the scar tissue, border region, and remote healthy myocardium regions, our cardiac fibrosis model will utilize varying cell ratios: pure iCF for the scar region, an iCM to iCF ratio of 1 : 3 for the border region, and an iCM to iCF ratio of 3 : 1 for the healthy myocardium (Fig. 6a). The differentiated cells were suspended in a collagen hydrogel with different ratios and consequently seeded into specified chambers in the microfluidic device.

To validate cell-patterning in our cardiac fibrosis model, immunostaining was performed using cell-specific biomarkers—troponin-T for iCMs and vimentin for iCFs. Fig. 6b and c demonstrates the cellular distribution in our cardiac fibrosis model: in the scar region, only vimentin (iCF marker) is present, while the border and health sections exhibit a higher expression of troponin-T (iCM marker). These immunostaining results confirm that our cardiac fibrosis model successfully replicates physiologically relevant cell patterning in cardiac fibrosis, with scar tissue

surrounded by a transitional border zone and connected to healthy myocardium.

The physical connectivity between regions allowed direct cell–cell communication through paracrine signaling and gap junctions, and indirect biomechanical interactions *via* the 3D hydrogel, establishing a relevant cardiac environment for spatially controlled macrophages and TGF-β introduction.

B. Macrophage with gradient distribution. To model the immune component in the post-MI fibrosis, we introduced macrophages with gradient spatial localization (Fig. 6d). Following MI, the death of numerous CMs leads to the release of damage-associated molecules, which subsequently recruit macrophages to the injury site.[21,22] These macrophages then produce inflammatory cytokines and chemokines,[23,24] initiating a fibrotic response essential for tissue repair. By introducing macrophages, our model can capture this early inflammatory phase of fibrosis, offering insights into how initial immune responses drive fibrotic progression.

We utilized the selective valve actuation system to introduce macrophages into the target cell chamber with an accumulating macrophage amount in the target site, as well as confining the distribution area of the macrophage within the fibrosis section. We first seeded the iCM and iCF into our device to generate a cardiac fibrosis model, while iCM is labeled with the green cell-tracker and iCF is labeled with red cell-tracker (Fig. 6e and f). Quantification of the iCM/iCF ratio revealed values of 1 : 2.75 in the border zone and 3.56 : 1 in the healthy region (Fig. 6g), closely matching the intended ratios of 1 : 3 and 3 : 1, respectively. Then, macrophages are labeled blue cell-tracker and introduced into our fibrosis model. Within our fibrosis mode, three outflows that related to the fibrosis sections (scar tissue and border zone) remain open and the macrophage-laden flow was guided into scar and fibrotic regions and accumulated within these regions. As shown in Fig. 6f, the final spatial distribution of macrophages mirrors the *in vivo* pattern—densely populated in the scar region and gradually reduced in adjacent tissue. The iMac density, calculated as the number of cells divided by the area, was measured at 0.18%, 0.07%, and 0.02% in the scar, border, and healthy sections, respectively, demonstrating a clear gradient distribution across the fibrosis model (Fig. 6g).

This introduction of immune cells with a gradient distribution marks a significant advancement over conventional fibrosis models, enabling investigation into early-stage immune-modulated fibrotic signaling and crosstalk between cardiac and immune cells within defined regions.

C. Benchmark: gradient concentration of TGF-β. TGF-β, a cytokine secreted predominantly by activated macrophages post-MI, plays a central role in driving fibroblast activation and ECM remodeling.[25,26] The concentration tends to be highest near regions of scar tissue where fibrotic activity is most intense, while the concentration is lower in border regions and much lower in healthy tissue.[27] Therefore, we aimed to introduce the TGF-β into our cardiac fibrosis model with such a gradient concentration to represent fibrotic activation in the absence of immune cell dynamics. By leveraging our microfluidic device's source-sink design and selective valve actuation, we established a stable TGF-β gradient, highest in the scar zone and gradually decreasing across the border and healthy regions (Fig. 6h).

Due to the difficulty of directly quantifying TGF-β concentrations *in situ*, we assessed the biological effect of TGF-β on iCFs *via* immunostaining. TGF-β is known to induce the activation of CFs into myo-CFs, which can be characterized by measuring the ratio of alpha-smooth muscle actin (α-SMA) and vimentin.[28] α-SMA is a specific protein marker of activated myo-CFs, with expression levels that increase significantly under activation conditions but remain generally low in normal fibroblast cultures. On the other hand, vimentin is a common protein marker of CFs. Therefore, by measuring the ratio of α-SMA to vimentin, we can indirectly estimate TGF-β concentrations across different regions in our model.

After seeding iCMs and iCFs mimicking cardiac fibrosis, we then flowed the TGF-β-loaded medium through introducing channel and direct the introduction of the TGF-β into the scar region. TGF-β gradually diffused across the whole cell chambers, leading to a gradient concentration within the fibrosis model. Then, the effects of TGF-β by comparing the ratio of alpha-SMA staining to vimentin across different tissue chambers were observed (Fig. 6i and j). All immunostaining images were acquired at the same exposure time, and the α-SMA/vimentin ratio was quantified based on fluorescence intensities within the regions of interest. Notably, the target scar tissue section showed the highest ratio is 0.90 ± 0.04, indicating of the highest concentration of TGF-β and most CFs were activated and transformed into myo-CFs. In other sections, the ratio is 0.63 ± 0.06 and 0.61 ± 0.05 due to the lower TGF-β concentration (Fig. 6k). As a control, we performed the same perfusion conditions using only media without TGF-β (Fig. S2) and quantified the α-SMA/vimentin ratio across three sections. The results showed no significant differences among the sections, confirming that fibrotic activation was specifically induced by TGF-β treatment. These results demonstrate that our model can reliably recreate region-specific fibrotic signaling, providing a control for comparison with immune cell-mediated effects.

D. Comparison with 2D cardiac fibrosis model. For comparison, we also developed a simple 2D cardiac fibrosis model by co-culturing iCMs and iCFs. However, 2D systems present significant limitations. Their fixed cell composition allows modeling of only a single section (*e.g.*, scar or healthy tissue) precluding investigation of regional interactions. In addition, biochemical treatments are uniformly applied. As shown in Fig. S3, macrophages in the 2D co-culture displayed uniform distribution, as indicated by CD14 staining. Similarly, TGF-β treatment could only be applied at a fixed concentration (or omitted entirely), without spatial modulation. Compared with the proposed 3D chip system,

these traditional 2D models lack flexibility and fail to recapitulate the complex spatial organization and microenvironment of *in vivo* cardiac fibrosis.

Discussion

Following MI, the crosstalk between immune cells (particularly macrophages) and cardiac cells is pivotal in orchestrating wound healing, and its dysregulation is strongly linked to excessive fibrosis and adverse cardiac remodeling. After MI, immune cells, such as macrophages, are recruited to specific areas of injury, where they engage in both the inflammatory and healing phases.[21,29] In the early inflammatory phase, monocyte-derived macrophages infiltrate the infarcted myocardium and adopt a pro-inflammatory phenotype, secreting cytokines such as tumor necrosis factor-alpha (TNF-α), interleukin-1 beta (IL-1β), and TGF-β that activate CFs into Myo-CFs.[30] These myofibroblasts contribute to ECM remodeling through the excessive production of collagen and fibronectin, ultimately leading to scar formation. As healing progresses, macrophages undergo a phenotypic shift toward the anti-inflammatory phenotype, releasing growth factors like IL-10 and TGF-β.[31,32] This phenotypic shift supports ECM remodeling, angiogenesis, and a transition from a fibrotic to a reparative environment. This dynamic spatial and temporal regulation of immune–cardiac interactions is critical in regulating the cardiac fibrosis following MI, impairing cardiac function and contributing to heart failure.

Most of the current mechanistic understanding of immune–cardiac cell crosstalk originates from rodent studies, which have inherent limitations due to species-specific differences and complexities in translating findings to human cardiovascular physiology. Additionally, conventional 2D co-culture models fail to adequately recapitulate the spatial heterogeneity and complex multicellular interactions that characterize the human heart's microenvironment following MI.

To overcome these limitations, we developed a 3D cardiac fibrosis-on-a-chip model that enables precise spatial patterning of scar, border, and healthy cardiac zones using engineered cell distributions. This was achieved be designing a valve-actuation system in the multi-layer microfluidic device for controlled macrophage gradient introduction. Unlike traditional co-culture systems that uniformly introduce immune cells, our device mirrors the spatial dynamics of macrophage infiltration observed *in vivo*—dense in scar regions and decreasing progressively toward healthy myocardium—thereby faithfully replicating post-MI inflammatory gradients and achieving a high level of complexity that rarely achieved in prior models.

Previous 2D co-culture systems, which typically involve mixing CMs, CFs and immune cells in a single culture well to model inflammatory cardiac conditions, allows the direct cell–cell connection and paracrine signaling. For example, a simple 2D co-culture of iMacs with iCMs to model COVID-19 myocarditis has shown that the presence of macrophages (*via* secreted IL-6 and TNF-α) caused CM reactive oxygen species accumulation and apoptosis and dramatically increased stress in the CMs.[33] Other studies have also co-cultured macrophages with iCM in transwells indicating different macrophage subtypes affect cardiomyocyte function and gene expression.[34] However, simple 2D co-cultures lack tissue-level architecture and fail to capture region–specific interactions or localized immune responses.

Conversely, 3D culture systems, such as cardiac spheroids, 3D printing, or microfluidic devices, have offered greater physiological relevance through defined tissue architectures. For instance, in recent 3D bioprinting studies, cell-laden bioinks are deposited in a programmed pattern to model cardiac fibrosis by designing tissues containing adjacent regions that mimic a fibrotic scar, border zone, and healthy myocardium.[35] Some microfluidics-based heart-on-a-chips co-cultured CMs or CFs and macrophages in adjacent microchannels separated by narrow connecting grooves to recreate inflammation-induced myocardial injury while enabling paracrine cytokines crosstalk.[36,37] Moreover, advanced systems integrated perusable vascular networks within cardiac microtissues. Lu *et al.* developed a vascularized cardiac chip perfused with immune cells, which replicated immune cell recruitment and the resultant contractile dysfunction observed in viral myocarditis.[38] Another recent study utilized the biowire model to co-culture human primitive macrophages with CM and CF, indicating that primitive macrophages enhanced cardiac tissue function by triggering iCM maturation, enhancing contractile force and improving relaxation kinetics.[39] Similarly, another study integrated human primitive macrophages and the biowire model with the endothelial network, indicating that primitive macrophages promoted the cardiac microvasculature development.[40] Each of these 3D models incorporated immune cells and tissue architecture to better recapitulate the complex fibrotic remodeling under inflammation *in vitro*. However, these platforms typically introduce immune cells uniformly, lacking precise control over immune cell localization and the accurate modeling of the spatially and temporally dynamic interactions between immune cells and cardiac cells that are critical in the progression of cardiac fibrosis.

Our unique three-layer microfluidic design addresses these critical gaps by recapitulating the distinct scar, border and healthy regions after fibrosis and utilizing the gradient introduction of macrophages to create a hyperinflammatory microenvironment, enabling the recapitulation of region–specific fibrotic responses under the influence of an immune gradient, closely mirroring the *in vivo* scenario after myocardial infarction. In our fibrosis-on-chip, macrophages are most concentrated in the engineered scar region and gradually decrease toward the healthy region, similar to the dominance of inflammatory cells in infarcted myocardium *in vivo*. Such spatial insights are supported by other gradient-

on-chip studies. For example, a recent "border-zone-on-a-chip" model was exposed to an oxygen gradient to specifically simulate an ischemic border zone, showing that distinct molecular responses in high-stress *vs.* low-stress regions.[41] Such oxygen gradient design replies on the gas permeability of PDMS and the oxygen concentration difference has also been widely applied in other organ-on-a-chip models.[42–44] Moreover, Nicolas Garcia-Seyda *et al.* used a microfluidic device with defined chemokine gradients to investigate naive T lymphocyte migration in response to chemokine gradient.[45] The results indicated that the naive T cells will directly migrate along a gradient of soluble cues. Similarly, Parvaneh Sardarabadi *et al.* developed a diffusion-based microfluidic chip to establish a stable interleukin-6 (IL-6) gradient across different cell chambers and examine immune cell migration dynamics.[46] By extending this gradient concept, our model significantly enhances physiological relevance for immune-mediated cardiac fibrosis research.

Our spatial cell-patterning strategy allows the exploration of cardiac cellular interactions under fibrotic conditions. We co-patterned CMs and CFs into 3D hydrogels with defined ratios, followed by seeding into separate tissue chambers to recreate the cellular architecture of fibrotic and healthy tissue regions *in vitro*. Scar tissue was recapitulated by seeding one chamber with a hydrogel containing solely CFs, while adjacent chambers were seeded with fibrotic tissue (CM–CF ratio 1 : 3) and healthy tissue (CM–CF ratio 3 : 1). Such spatial organization enables physical contact during the culturing, facilitating direct bioelectrical and biochemical interactions between scar tissue and fibrotic and healthy tissue, thereby facilitating the study of pathological changes in cell communication, such as disrupted paracrine signaling and gap junction dysfunction under fibrotic conditions. Additionally, our cardiac fibrosis-on-a-chip model can integrate with other measuring methodologies including microscope imaging, microelectrode recording and RNA extraction from specific regions. These measuring capabilities enable a comprehensive analysis of how fibrosis-induced changes impact cell-to-cell connections, signaling pathways, and overall contractile function, making this model a valuable tool for understanding fibrosis mechanisms and testing targeted therapeutic approaches.

In addition to structural patterning, we further enhanced physiological relevance by incorporating gradient delivery of macrophages to mimic the localized immune dynamics observed after MI. *In vivo*, macrophages are recruited to injury sites where they engage in both the inflammatory and healing phases.[21,29] Initially, macrophages adopt a pro-inflammatory M1 phenotype, releasing cytokines such as TNF-α,[47] IL-1, and IL-6, which activate nearby fibroblasts and promote ECM deposition to stabilize the injured tissue.[30] As healing progresses, macrophages undergo a phenotypic shift toward the M2, anti-inflammatory phenotype, releasing growth factors like IL-10 and TGF-β.[31,32] This phenotypic shift supports ECM remodeling, angiogenesis, and a transition from a fibrotic to a reparative environment. By introducing immune cells with defined spatial localization to a cardiac fibrosis model, we can replicate the localized inflammatory and healing phase that modulates fibrosis. This approach allows for the investigation of how early immune signals drive fibrosis progression, ECM production, and subsequent tissue remodeling.

In parallel with immune regulation, biochemical signaling is another key mediator during fibrosis progression. Biochemical molecules including TGF-β, interleukins (*e.g.*, IL-1 and IL-6), and growth factors,[23,24,48] all play an important role in cardiac fibrosis and pathological cell interactions. For example, *in vivo*, the high TGF-β concentrations near the scar tissue led to a higher level of CF activation and profibrotic markers expression, while cells further from scar tissue experience less activation due to the lower TGF-β concentrations. Similarly, interleukins like IL-1 and IL-6, which are often elevated following myocardial injury, mediate inflammatory responses by recruiting immune cells to the injured area and promoting further fibroblast activation.[23,48] Introducing these molecules at varying concentrations within the fibrosis model allows for the simulation of localized inflammation and fibrotic responses, as seen *in vivo*, where inflammation peaks near the scar and diminishes in surrounding regions. Additionally, vascular endothelial growth factor (VEGF) and other angiogenic factors are crucial for replicating the repair and remodeling processes in the border and remote zones.[49,50] VEGF promotes the vascular formation which is crucial for delivering oxygen and nutrients during tissue repair process. Incorporating these molecules in a spatially controlled manner enables the model to replicate the intricate interplay of inflammatory, profibrotic, and reparative processes across different cardiac regions. This approach not only allows the study of region–specific responses to cardiac fibrosis but also allows for the testing of therapeutic interventions within distinct cardiac zones, paving the way for more precise and effective treatments. Despite its innovative features, our model has inherent limitations. First, the fabrication and operation of a three-layer microfluidic co-culture with multiple cell types requires specialized expertise. The added complexity can introduce variability, particularly in ensuring consistent patterning of the "scar" *vs.* "healthy" regions in each experiment, may be challenging. Furthermore, our current model focuses primarily on macrophages, neglecting the full involvement of immune cells (*e.g.*, neutrophils, T-cells) and endothelial interactions critical in the *in vivo* inflammatory cascade post-MI. This is a conscious trade-off to maintain a manageable model, but it is an area for future enhancement.

Nevertheless, our immune-integrated cardiac fibrosis chip provides broader implications. The device provides a more physiologically relevant model for drug discovery. Anti-fibrotic or immunomodulatory therapies can be applied in our system to see how they affect not just a single cell type in isolation, but the multicellular response across different regions of damaged heart tissue. Moreover, this cardiac

fibrosis-on-chip is extensible to other cardiac pathologies where the immune system plays a role, such as myocarditis, by adjusting the cell patterning and stimuli.

In conclusion, our 3D cardiac fibrosis-on-a-chip model effectively integrates cardiac cell interactions, spatial organization, and precise immune cell gradients. This physiologically relevant system significantly enhances the accuracy and relevance of modeling post-MI cardiac fibrosis, serving as a robust model for mechanistic studies and therapeutic screenings in conditions that closely mimic human disease states.

Conflicts of interest

There are no conflicts to declare.

Data availability

The data supporting this article have been included as part of the supplementary information (SI). Supplementary information is available. See DOI: https://doi.org/10.1039/d5lc00469a.

References

1 S. S. Virani, *et al.*, Heart Disease and Stroke Statistics—2021 Update, *Circulation*, 2021, **143**, e254–e743.
2 E. Tzahor and S. Dimmeler, A coalition to heal—the impact of the cardiac microenvironment, *Science*, 2022, **377**, eabm4443.
3 F. J. Carrillo-Salinas, N. Ngwenyama, M. Anastasiou, K. Kaur and P. Alcaide, Heart Inflammation: Immune Cell Roles and Roads to the Heart, *Am. J. Pathol.*, 2019, **189**, 1482–1494.
4 A. Deb, Cell-cell interaction in the heart via Wnt/β-catenin pathway after cardiac injury, *Cardiovasc. Res.*, 2014, **102**, 214–223.
5 N. G. Frangogiannis, The Extracellular Matrix in Ischemic and Nonischemic Heart Failure, *Circ. Res.*, 2019, **125**, 117–146.
6 H. K. Awada, M. P. Hwang and Y. Wang, Towards comprehensive cardiac repair and regeneration after myocardial infarction: Aspects to consider and proteins to deliver, *Biomaterials*, 2016, **82**, 94–112.
7 M. Hulsmans, *et al.*, Macrophages Facilitate Electrical Conduction in the Heart, *Cell*, 2017, **169**, 510–522.e20.
8 C. P. Soares, *et al.*, 2D and 3D-Organized Cardiac Cells Shows Differences in Cellular Morphology, Adhesion Junctions, Presence of Myofibrils and Protein Expression, *PLoS One*, 2012, **7**, e38147.
9 J. Veldhuizen, *et al.*, Cardiac ischemia on-a-chip to investigate cellular and molecular response of myocardial tissue under hypoxia, *Biomaterials*, 2022, **281**, 121336.
10 E. Y. Wang, *et al.*, Biowire Model of Interstitial and Focal Cardiac Fibrosis, *ACS Cent. Sci.*, 2019, **5**, 1146–1158.
11 M. Feyen, *et al.*, Metabolic Maturation Media Improve Physiological Function of Human iPSC-Derived Cardiomyocytes, *Cell Rep.*, 2020, **32**, 107925.
12 J. Zhang, *et al.*, Functional cardiac fibroblasts derived from human pluripotent stem cells via second heart field progenitors, *Nat. Commun.*, 2019, **10**, 2238.
13 B. van Wilgenburg, C. Browne, J. Vowles and S. A. Cowley, Efficient, Long Term Production of Monocyte-Derived Macrophages from Human Pluripotent Stem Cells under Partly-Defined and Fully-Defined Conditions, *PLoS One*, 2013, **8**, e71098.
14 J. Gao, Z. Xu, R. Han, Z. Qi and G. Han, Refinement of Hyperelastic Models Based on Tension and Compression Experiments of Polydimethylsiloxane (PDMS), *Mech. Solids*, 2024, **59**, 955–965.
15 M. Miles, *et al.*, Flattening of Diluted Species Profile via Passive Geometry in a Microfluidic Device, *Micromachines*, 2019, **10**, 839.
16 I. Zervantonakis, *et al.*, Concentration gradients in microfluidic 3D matrix cell culture systems, *Int. J. Micro-Nano Scale Transp.*, 2010, **1**, 27–36.
17 H. Chen, T. Yamada and M. Faghri, Measurement of Burst Pressure of Capillary Burst Valve, *International Conference on Nanochannels, Microchannels, and Minichannels*, 2010, vol. 54501.
18 G. Fu and W. Kuang, Optimal Geometric Multigrid Preconditioners for HDG-P0 Schemes for the reaction-diffusion equation and the Generalized Stokes equations, *ESAIM:Math. Modell. Numer. Anal.*, 2023, **57**, 1553–1587.
19 G. Fu and W. Kuang, hp-Multigrid Preconditioner for a Divergence-Conforming HDG Scheme for the Incompressible Flow Problems, *J. Sci. Comput.*, 2024, **100**, 16.
20 B. W. Ellis, A. Acun, U. I. Can and P. Zorlutuna, Human iPSC-derived myocardium-on-chip with capillary-like flow for personalized medicine, *Biomicrofluidics*, 2017, **11**, 024105.
21 Y. Jian, *et al.*, Crosstalk between macrophages and cardiac cells after myocardial infarction, *Cell Commun. Signaling*, 2023, **21**, 109.
22 J. Yap, *et al.*, Macrophages in cardiac remodelling after myocardial infarction, *Nat. Rev. Cardiol.*, 2023, **20**, 373–385.
23 M. Huang, D. Yang, M. Xiang and J. Wang, Role of interleukin-6 in regulation of immune responses to remodeling after myocardial infarction, *Heart Failure Rev.*, 2015, **20**, 25–38.
24 M. Jung, *et al.*, IL-10 improves cardiac remodeling after myocardial infarction by stimulating M2 macrophage polarization and fibroblast activation, *Basic Res. Cardiol.*, 2017, **112**, 33.
25 M. Bujak and N. G. Frangogiannis, The role of TGF-β Signaling in Myocardial Infarction and Cardiac Remodeling, *Cardiovasc. Res.*, 2007, **74**, 184–195.
26 N. G. Frangogiannis, The role of transforming growth factor (TGF)-β in the infarcted myocardium, *J. Thorac. Dis.*, 2017, **9**, S52–S63.
27 K. W. Finnson, S. McLean, G. M. Di Guglielmo and A. Philip, Dynamics of Transforming Growth Factor Beta Signaling in Wound Healing and Scarring, *Adv. Wound Care*, 2013, **2**, 195–214.
28 S. W. M. van den Borne, *et al.*, Myocardial remodeling after infarction: the role of myofibroblasts, *Nat. Rev. Cardiol.*, 2010, **7**, 30–37.

29 N. G. Frangogiannis, The inflammatory response in myocardial injury, repair, and remodelling, *Nat. Rev. Cardiol.*, 2014, **11**, 255–265.
30 Y. Hu, *et al.*, Class A scavenger receptor attenuates myocardial infarction-induced cardiomyocyte necrosis through suppressing M1 macrophage subset polarization, *Basic Res. Cardiol.*, 2011, **106**, 1311–1328.
31 G. Bajpai, *et al.*, The human heart contains distinct macrophage subsets with divergent origins and functions, *Nat. Med.*, 2018, **24**, 1234–1245.
32 H. Zhang, *et al.*, Self-Maintenance of Cardiac Resident Reparative Macrophages Attenuates Doxorubicin-Induced Cardiomyopathy Through the SR-A1-c-Myc Axis, *Circ. Res.*, 2020, **127**, 610–627.
33 L. Yang, *et al.*, An Immuno-Cardiac Model for Macrophage-mediated Inflammation in COVID-19 Hearts, *Circ. Res.*, 2021, **129**, 33–46.
34 E. A. Wrona, B. Sun, S. Romero-Torres and D. O. Freytes, Effects of polarized macrophages on the in vitro gene expression after Co-Culture of human pluripotent stem cell-derived cardiomyocytes, *J. Immunol. Regener. Med.*, 2019, **4**, 100018.
35 G. Basara, L. E. Celebi, G. Ronan, V. Discua Santos and P. Zorlutuna, 3D bioprinted aged human post-infarct myocardium tissue model, *Health Sci. Rep.*, 2024, **7**, e1945.
36 Z. Gao, *et al.*, A microfluidic coculture model for mapping signaling perturbations and precise drug screening against macrophage-mediated dynamic myocardial injury, *Acta Pharm. Sin. B*, 2024, **14**, 5393–5406.
37 P. Li, *et al.*, A Microfluidic Cell Co-Culture Chip for the Monitoring of Interactions between Macrophages and Fibroblasts, *Biosensors*, 2023, **13**, 70.
38 R. X. Z. Lu, *et al.*, Cardiac tissue model of immune-induced dysfunction reveals the role of free mitochondrial DNA and the therapeutic effects of exosomes, *Sci. Adv.*, 2024, **10**, eadk0164.
39 H. Hamidzada, *et al.*, Primitive macrophages induce sarcomeric maturation and functional enhancement of developing human cardiac microtissues via efferocytic pathways, *Nat. Cardiovasc. Res.*, 2024, **3**, 567–593.
40 S. Landau, *et al.*, Primitive macrophages enable long-term vascularization of human heart-on-a-chip platforms, *Cell Stem Cell*, 2024, **31**, 1222–1238.e10.
41 M. L. Rexius-Hall, *et al.*, A myocardial infarct border-zone-on-a-chip demonstrates distinct regulation of cardiac tissue function by an oxygen gradient, *Sci. Adv.*, 2022, **8**, eabn7097.
42 X. Li, S. M. George, L. Vernetti, A. H. Gough and D. L. Taylor, A glass-based, continuously zonated and vascularized human liver acinus microphysiological system (vLAMPS) designed for experimental modeling of diseases and ADME/TOX, *Lab Chip*, 2018, **18**, 2614–2631.
43 R. Mahdavi, *et al.*, Design, fabrication, and characterization of a user-friendly microfluidic device for studying liver zonation-on-chip (ZoC), *Biomed. Microdevices*, 2025, **27**, 8.
44 H.-H. Hsu, *et al.*, Studying sprouting angiogenesis under combination of oxygen gradients and co-culture of fibroblasts using microfluidic cell culture model, *Mater. Today Bio*, 2023, **21**, 100703.
45 N. Garcia-Seyda, *et al.*, Naive T lymphocytes chemotax long distance to CCL21 but not to a source of bioactive S1P, *iScience*, 2023, **26**, 107695.
46 P. Sardarabadi, K.-Y. Lee, W.-L. Sun and C.-H. Liu, Immune response to IL6 gradient in a diffusion-based microfluidic labchip, *Sens. Actuators, B*, 2024, **417**, 136141.
47 X. Yu, *et al.*, Mechanism of TNF-α autocrine effects in hypoxic cardiomyocytes: Initiated by hypoxia inducible factor 1α, presented by exosomes, *J. Mol. Cell. Cardiol.*, 2012, **53**, 848–857.
48 A. Saxena, *et al.*, IL-1 Induces Proinflammatory Leukocyte Infiltration and Regulates Fibroblast Phenotype in the Infarcted Myocardium, *J. Immunol.*, 2013, **191**, 4838–4848.
49 Z. Tao, *et al.*, Coexpression of VEGF and angiopoietin-1 promotes angiogenesis and cardiomyocyte proliferation reduces apoptosis in porcine myocardial infarction (MI) heart, *Proc. Natl. Acad. Sci. U. S. A.*, 2011, **108**, 2064–2069.
50 T. Zhao, *et al.*, VEGF-C/VEGFR-3 pathway promotes myocyte hypertrophy and survival in the infarcted myocardium, *Am. J. Transl. Res.*, 2015, **7**, 697–709.